Available online at www.sciencedirect.com
SCIENCE DIRECT®
Sensors and Actuators A 116 (2004) 369–377
SENSORS AND ACTUATORS A PHYSICAL
www.elsevier.com/locate/sna

Demonstration and characterization of PZT thin-film sensors and actuators for meso- and micro-structures

Yi-Chu Hsu [a], Chia-Che Wu [b], Cheng-Chun Lee [b], G.Z. Cao [c], I.Y. Shen [b,*]

[a] *Department of Mechanical Engineering, Southern Taiwan University of Technology, Tainan 710, Taiwan*
[b] *Department of Mechanical Engineering, University of Washington, Box 352600, Seattle, WA 98195-2600, USA*
[c] *Department of Material Science and Engineering, University of Washington, Seattle, WA 98195-2120, USA*

Received 31 January 2004; received in revised form 22 May 2004; accepted 23 May 2004
Available online 2 July 2004

Abstract

Recent development of next-generation medical devices, such as endoscopes and hearing aids, call for PZT (lead zirconate titanate oxide) thin-film sensors and actuators with thickness in the range of 1–30 μm to enhance actuation strength and sensor sensitivity. Currently, sol–gel derived PZT films often have thickness less than 0.2 μm per coating. Moreover, thermal stresses in the films limit the crack-free area to less than 1 mm^2. This paper has four specific goals. The first goal is to demonstrate an improved sol–gel process using rapid thermal annealing and a diluted sealant coating. The resulting thickness can reach 2 μm in three coatings with a crack-free area as large as 5 mm × 5 mm. The second goal is to characterize piezoelectric properties of the fabricated PZT films experimentally. The resulting piezoelectric constant d_{33} is 120 pC/N and the dielectric constant ranges from 200 to 400. The third goal is to demonstrate the use of the PZT thin film as a calibrated sensor. The specimen is a silicon cantilever (30 mm × 7.5 mm × 0.4 mm) with a PZT thin film (4 mm × 4 mm × 1 μm). Moreover, a tiny shaker excites the cantilever at the fixed end, and a charge amplifier detects the charge accumulated in the PZT film. In the meantime, a laser vibrometer measures the deflection of the cantilever at three points along the PZT film, from which the strain is calculated using Euler–Bernoulli beam theory. Comparison of the strain and the charge amplifier voltage determines the calibration constant of the PZT thin-film sensor. The last goal is to demonstrate the use of the PZT thin film as a powerful actuator through active vibration control. In experiments, a tiny bulk PZT patch is first glued to the silicon cantilever. A function generator drives the bulk PZT simulating a source of disturbance exciting the silicon cantilever. In the meantime, a laser Doppler vibrometer (LDV) measures velocity of the cantilever tip. With a phase shifter as the controller, the LDV measurement is fed back to the PZT thin-film actuator to actively control the cantilever vibration. To evaluate the effectiveness of the active vibration control, a spectrum analyzer measures the frequency response functions (FRF) from the bulk PZT voltage to the LDV response. Experimental results show that the simple active vibration control scheme can reduce resonance amplitude of the first bending mode by 66%.

Keywords: PZT thin films; Sol–gel process; Sensor calibration; Active vibration control

1. Introduction

Lead zirconate titanate oxide ($PbZr_{1-x}Ti_xO_3$ or PZT) is a piezoelectric material widely used as sensors and actuators for bulk structures. Advantages of PZT-based devices include high frequency bandwidth, fast response, and high sensitivity. Miniaturization of PZT-based devices will not only perfect many existing products, but also open vast new applications. Here are several promising examples. PZT-based active recording head sliders are being tested by the disk drive industry to enhance data density by orders of magnitude [1]. PZT-based microactuators can lead to miniature ultrasonic surgical tools to remove damaged cells and cardiovascular deposition. As a result, surgeries could become significantly less invasive, and patients would have a faster recovery. PZT-based microactuators can also serve as fuel injectors for micro-engines that could potentially replace traditional batteries as an alternative power source. PZT-based microactuators can also power sensing devices (e.g., acoustic wave sensors) to detect specific molecules, proteins, and bacteria in chemical and biological agents [2–4].

As a concrete example, recent development of next-generation endoscopes calls for high-performance PZT thin-film actuators. Traditional endoscopes have large di-

* Corresponding author. Tel.: +1-206-5435718; fax: +1-206-6858047.
E-mail address: ishen@u.washington.edu (I.Y. Shen).

0924-4247/$ – see front matter © 2004 Elsevier B.V. All rights reserved.
doi:10.1016/j.sna.2004.05.024

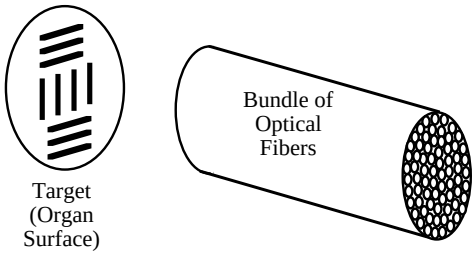

Fig. 1. Setup of current endoscopes in use.

ameter (about the size of a vitamin pill), because they use a bundle of optical fibers to image organ surfaces; see Fig. 1. As a result, traditional endoscopes have two severe drawbacks. First, traditional endoscopes can only probe organs with large openings, such as stomachs. Moreover, use of endoscopes requires general anesthesia. The second drawback is that traditional endoscopes cannot be sterilized because of the optical fibers. The general practice is to disinfect the endoscopes. Therefore, there is a strong need in the medical community to develop minute endoscopes for sensitive tracts (e.g., bronchia) and disposable endoscopes for sanitary reasons.

Fig. 2 shows the central piece of a next-generation, minute, disposable endoscope [5]. The overall size of the endoscope is less than 1 mm in diameter and 5 mm in length. The major component is a *single* optical fiber; therefore, the size of the endoscopes can be dramatically reduced. At the end of the optical fiber, a minute resonator drives the optical fiber scanning through the two-dimensional surface to obtain the image. (Dimension specification of the resonator is less than 800 μm in diameter.) A major technical challenge is to find a minute actuator that has large enough actuation strength while scanning at a high frequency, such as 5–15 kHz or more. According to Krulevitch et al. [6], there are four types of microactuators: thermal, shape-memory-alloy (SMA), electrostatic, and piezoelectric (specifically PZT). Thermal and SMA actuators have low frequency bandwidth [6] (<1 kHz), whereas electrostatic and PZT actuators have high frequency bandwidth (>1 kHz). Moreover, electrostatic actuators have much smaller actuation force and energy density than PZT films (3.4×10^3 J/m^3 for electrostatic actuators versus 1.2×10^5 J/m^3 for PZT [6]). Based on these considerations, the best design choice

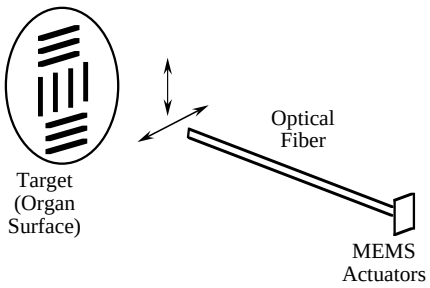

Fig. 2. Setup of next-generation endoscopes.

for the next-generation scanning endoscopes is PZT microactuators.

Despite the needs, miniaturization of bulk PZT devices into millimeter or micron ranges is not trivial [7–10]. Traditional bulk PZT often appears as thin patches with thickness not less than 80 μm. In contrast, PZT microactuators call for PZT films with thickness less than 80 μm. In designing PZT microactuators, thickness of the PZT films is a critical parameter. In general, thicker PZT films lead to larger actuation strength and higher frequency bandwidth. (This is because the resistance R and the capacitance C of the PZT film form a low-pass filter with a cutoff frequency $1/RC$. As the film thickness increases, capacitance C decreases and the bandwidth increases.) However, thicker PZT films will require larger voltage (and power) to actuate. Also, too thick a PZT film could lead to poor aspect ratios between the PZT film and the substrate hurting the performance of the PZT microactuator.

To distinguish films of different thickness, we will use the following terminology. First, PZT films are called "super-thin films", if the film thickness is less than 1 μm. When the film thickness is between 1 and 30 μm, the PZT films are called "thin films". When the film thickness is over 30 μm, the films are called "thick films". Currently, successful research results are primarily for PZT super-thin films [11–13], and the film area is usually less than 1 mm^2. For thick PZT films, they can be fabricated by conventional tape-casting using slurry made of nano-PZT particles [14] for example. For PZT thin films, successful fabrication and processing of the films remain open thus far.

To identify a feasible way to fabricate PZT thin films, let us briefly review the fabrication processes of PZT films. Currently, successful processes of PZT films include sputtering [15–19], direct bonding [20,21], screen printing [22,23], metallorganic chemical vapor deposition (MOCVD) [24], and sol–gel processing [25–31]. (Also, pulsed laser deposition [32,33] could be a possible way to make PZT films.) So far, MOCVD and sol–gel processing are proven to be the most promising techniques for the fabrication of PZT thin films. MOCVD offers several advantages including conformal coverage, columnar micro-structures, and no need for post-deposition annealing [24]. In comparison, sol–gel processing offers three unfair advantages. First, it is easy to control the stoichiometric chemical composition of PZT films. This is extremely important for complex oxides such as PZT, because their physical properties strongly depend on the precise control of the chemical composition. Second, sol–gel processing is inexpensive, due to its 100% usage of precursors. Third, sol–gel processing is suitable for mass production and compatible with device fabrication processes. Based on these considerations, it is more beneficial to fabricate PZT thin films using sol–gel processing. Nevertheless, there are tremendous challenges to overcome.

The first challenge is the presence of cracks. Since PZT is a ceramic, its coefficient of thermal expansion (CTE) is very different from that of metal electrodes. As a re-

sult, substantial thermal stresses develop between the PZT and its metal electrodes during sintering cracking the PZT films. The presence of cracks can not only short-circuit the top and bottom electrodes, but also cause aging and fracture of PZT films. The second challenge is film thickness. Currently, PZT thin-film technology can offer a crack-free area about 1 mm^2 with film thickness ranging from 15 to 100 nm [11–13]. Therefore, multiple coatings are necessary to reach a thickness more than 1 μm. Multiple coating is not only time-consuming, but also substantially increases the chance for cracks. Other challenges include stability of bottom electrodes [34–37] and sintering temperature [38,39].

Motivated by the needs for stronger PZT thin films for meso- and micro-devices, this paper is to demonstrate an improved sol–gel process to fabricate PZT thin-film sensors and actuators. The PZT films have thickness in the range of 1–2 μm in three coatings, and the film area can be as large as 5 mm × 5 mm. The paper consists of four parts. The first part is to describe the sol–gel processes leading to the improved PZT films. The second part is to characterize material properties of the PZT films, such as piezoelectric constant and dielectric constant. The third part is to calibrate the PZT films as a sensor using charge amplifier and a laser Doppler vibrometer (LDV). The fourth part is to demonstrate the PZT films as an effective actuator through actively controlling vibration of a silicon cantilever beam.

2. Fabrication of PZT thin films

Fig. 3 shows a typical sol–gel process to fabricate PZT films. The first step is to deposit the bottom electrode on the silicon substrate. The second step is to dip-coat or spin-coat PZT sol onto the substrate. (PZT sol consists of non-soluble Pb, Zr, and Ti nano-clusters dispersed in solvent; see Appendix A for a recipe.) As the solvent evaporates from the sol, the condensation and hydrolysis process facilitates cross-linking of individual clusters in PZT sol resulting in the sol–gel transition. Third, the PZT/silicon structure is sintered at high temperature to densify the PZT film and form the desired crystalline phase. The sintering temperature ranges from 600 to 700 °C, and the sintering time can last from 4 to 6 h. Finally, the top electrode is deposited. Successful fabrication results in crack-free and well-adhered PZT films.

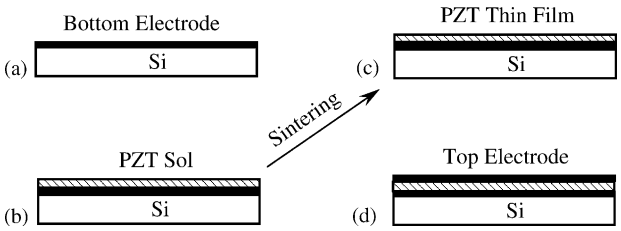

Fig. 3. Sol–gel process to fabricate PZT thin films.

To increase the thickness of PZT films, we primarily follow the procedure shown in Fig. 3 but optimize some process parameters. The silicon substrate is first oxidized in a furnace at 1045 °C for 2 h to grow a SiO_2 layer of 500 nm thick. Then a layer of silicon nitride of 200 nm thick is deposited by LPCVD (low-pressure chemical vapor deposition).

The bottom electrode consists of Pt and Ti layers with thickness of 100 and 50 nm, respectively. The bottom electrode is deposited via evaporation. The use of Pt as bottom electrode is very desirable, because it forms a good diffusion barrier preventing Pb from migrating into the silicon substrate. The Ti layer is to serve as an adhesion layer.

With the PZT sol recipe shown in Appendix A, the silicon substrate is dip-coated or spin-coated three times. For the first two coatings, the sintering temperature is 650 °C for 15 min. For the third coating, the sol is diluted 50% by acetic

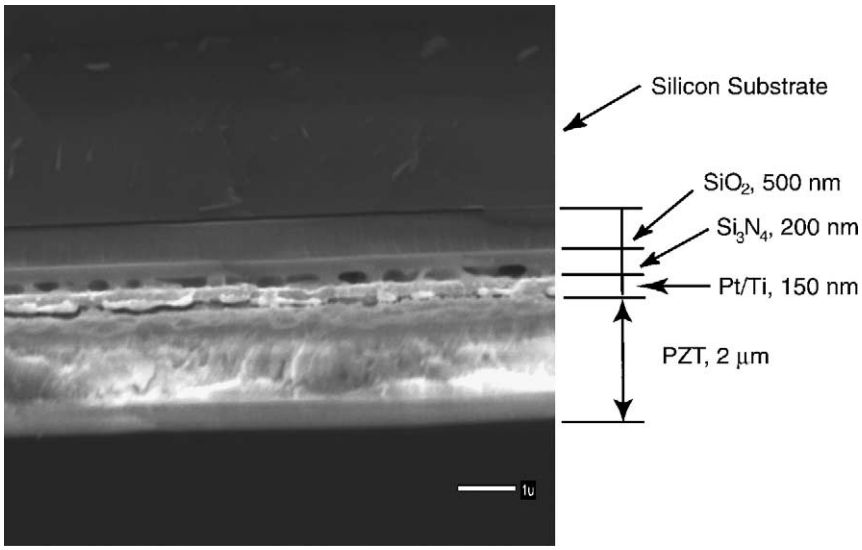

Fig. 4. SEM photo of the PZT thin film (cross-sectional view).

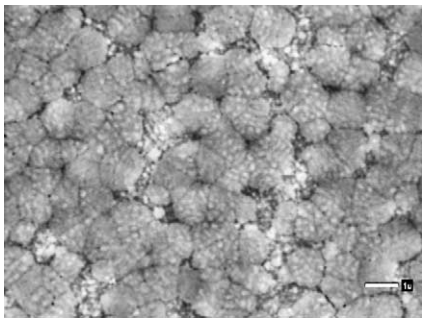

Fig. 5. SEM photo of the PZT thin film (top view).

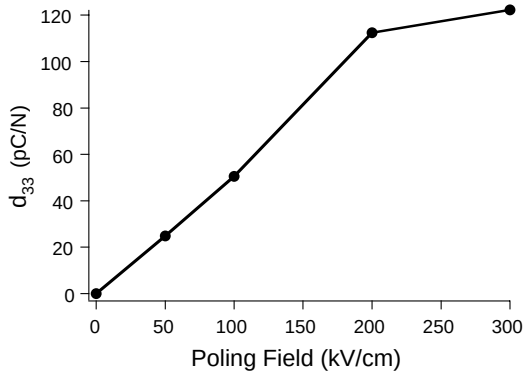

Fig. 6. Measured piezoelectric constant as a function of electric field.

acid and sintering temperature is 450 °C for 10 min. The philosophy is to use rapid thermal annealing for the first two coatings to reduce thermal stresses. The third coating with diluted sol is to seal possible cracks formed in previous coatings. With different process parameters (e.g., speed of the spin coating), the thickness of the PZT film can range from 1 to 2 μm (i.e., roughly 330–660 nm per coating). Fig. 4 shows the cross-sectional view of a PZT film with thickness around 2 μm through SEM. Moreover, the PZT film surface is crack-free and smooth as seen from the SEM photo; see Fig. 5. Also, X-ray diffraction of the PZT films shows that the films have the desired perovskite crystalline phase.

Finally, the top electrode consisting of Au and Cr layers is deposited through evaporation. The thickness of the Au and Cr layers is 50 and 20 nm, respectively. The size of the electrode (i.e., effective area of the PZT film) can be as large as 5 mm × 5 mm without short-circuiting the PZT film. Compared with existing literature, this sol–gel process has substantially improved the thickness and crack-free area of PZT thin films. The key to this improvement is the use of rapid thermal annealing and diluted coating.

3. Material properties of the films

Following the procedure published in [40], we measured dielectric constant ε_r and piezoelectric constant d_{33} of the PZT films. For dielectric constant, Table 1 shows some measurements at 1 kHz and 1 MHz for specimens from different batches before poling. As expected, some batches are better than the others. In general, the dielectric constant at 1 kHz ranges from 300 to 400. For piezoelectric constant d_{33}, we poled the specimen with voltage ranging from 0 to 30 V. Each poling step lasted for 30 min at room temperature. Assuming that the film thickness is 1 μm, the resulting electric field would range from 0 to 300 kV/cm. As shown in Fig. 6, the measured d_{33} saturates around 120 pC/N, when the electric field exceeds 200 kV/cm. The measured dielectric constant and piezoelectric constants are comparable with those published in the literature of PZT thin films [11–13].

Table 1
Experimental results to measure dielectric constant ε_r

	Batch 1		Batch 2			Batch 3		
	1[a]	2[a]	3[a]	4[a]	5[a]	6[a]	7[a]	8[a]
Area (mm^2)	4	4	9	9	9	4	4	4
Thickness (μm)	1	1	1	1	1	1	1	1
ε_r, 1 kHz	178	292	314	324	340	410	389	378
ε_r, 1 MHz	184	187	316	300	300	380	371	352

[a] Case numbers.

4. PZT thin films as sensors

Fig. 7 shows the setup to calibrate the PZT films as a sensor. The experimental setup consists of a silicon cantilever (30 mm × 7.5 mm × 0.4 mm) clamped to an AVC-712A01 piezoelectric actuator (made by PCB Piezotronics, Inc.). The silicon cantilever has a PZT film (4 mm × 4 mm × 1 μm), and the AVC piezoelectric actuator excites the silicon cantilever deforming the PZT film. A charge amplifier detects the charge accumulated in the PZT film. Then a spectrum analyzer processes the charge amplifier's output voltage to obtain a frequency spectrum; see the solid line in Fig. 8. Note that the measurement from the charge amplifier refers to the right axis in Fig. 8. Moreover, the first resonance

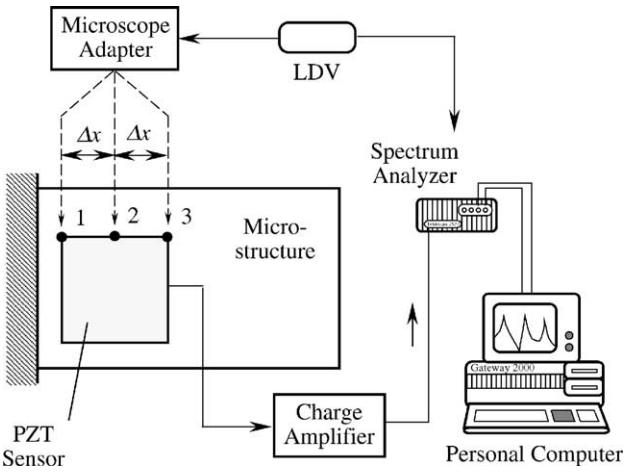

Fig. 7. Experimental setup to calibrate PZT thin film as a sensor.

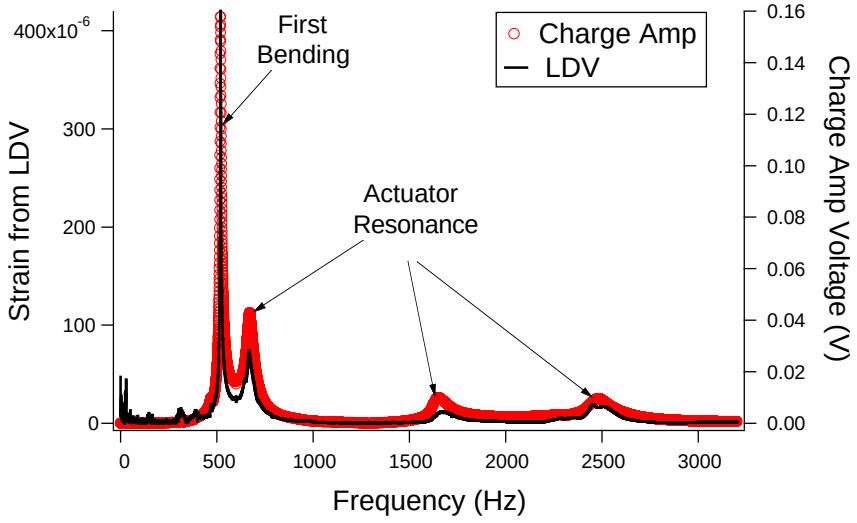

Fig. 8. Spectrum of PZT thin-film sensor from an LDV and a charge amplifier.

peak at 520 Hz is the first bending mode of the cantilever. The other peaks in Fig. 8 are resonance from AVC piezoelectric actuator. Before the experiment, the charge amplifier is adjusted so that its corner frequency is well below the first resonance frequency 520 Hz. Consequently, all the resonance peaks in Fig. 8 are amplified uniformly across the frequency and are proportional to the strain developed in the PZT thin film. Nevertheless, a calibration constant must be determined in order to relate the voltage to the strain numerically.

To obtain the calibration constant, we use a laser Doppler vibrometer (LDV) setup shown in Fig. 7. Let us first denote three points along the PZT film as 1, 2, and 3 in Fig. 7. These points are evenly spaced with distance $\Delta x = 2\,\text{mm}$. Then the LDV measures the deflection w_1, w_2, and w_3 of the cantilever at points 1, 2, and 3. According to Euler–Bernoulli beam theory, the curvature κ_2 of the cantilever at point 2 is approximated as

$$\kappa_2 \approx \frac{w_1 - 2w_2 + w_3}{(\Delta x)^2} \tag{1}$$

Moreover, the normal strain of the PZT film is $\varepsilon = \kappa_2 h/2$, where h is the thickness of the cantilever. The normal strain obtained through LDV measurements is also shown in Fig. 8 as comparison (referring to the left axis). The measured strain and the charge amplifier voltage agree very well with each other in both frequency and amplitude. By matching the resonance amplitudes at 520 Hz from the LDV and charge amplifier, calibration constant is $2.625 \times 10^{-3}\,\text{V}^{-1}$.

There are two things worth noting. First, the calibration constant $2.625 \times 10^{-3}\,\text{V}^{-1}$ is only valid at 520 Hz. This is because the relationship between the charge amplifier voltage and the strain is not exactly a constant. Instead, it depends on the frequency. Theoretically, if the PZT film is modeled as a one-dimensional continuum, the charge amplifier voltage V and the strain s satisfy the following relation:

$$\frac{V(\omega)}{s(\omega)} = \frac{EAd_{31}}{C}\mu \tag{2}$$

where E, A, d_{31} and C are the Young's modulus, area, piezoelectric constant, and capacitance of the PZT film, respectively. Moreover, μ is the gain of the charge amplifier (i.e., the ratio of the charge amplifier voltage to the open-loop voltage of the PZT film), which is around 4.4 in this experiment. Since d_{31} and dielectric constant are frequency dependent [41–44], it is natural that the calibration is frequency dependent. Therefore, it is more precise to state that the calibration constant is $2.625 \times 10^{-3}\,\text{V}^{-1}$ at 520 Hz.

Second, the calibration method described in Fig. 7 is independent of boundary conditions. Measuring charge generated from a PZT film is a common way to measure transverse piezoelectric coefficient e_{31}. Traditional methods to measure e_{31} include the following steps. First, PZT film is deposited on specimens that take the form of cantilevers [45], simply supported beams [46], or plates [47]. Second, a known load is applied to the specimens and the charge accumulated in the PZT film is measured. According to mechanics of materials, one can calculate the strain developed in the film assuming perfect boundary conditions (e.g., fixed) as in [45–47]. The ratio of the measured charge to the calculated strain gives e_{31} of the film. Since the real boundary conditions of the specimen are not perfect and cannot be modeled accurately, the strain and e_{31} calculated from the perfect boundary conditions often inherit some degrees of inaccuracy. In contrast, the use of curvature formula (1) in this paper does not require use of any boundary conditions at all.

5. PZT thin films as actuators—active vibration control

The experiments on active vibration control consist of several steps. The first step is to identify resonance fre-

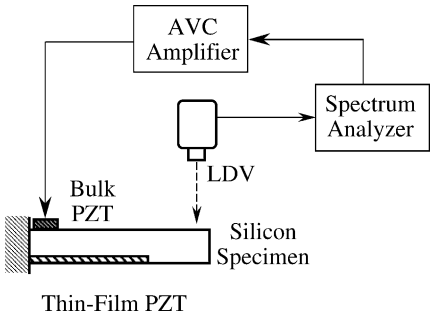

Fig. 9. Experimental setup to identify system resonance frequencies.

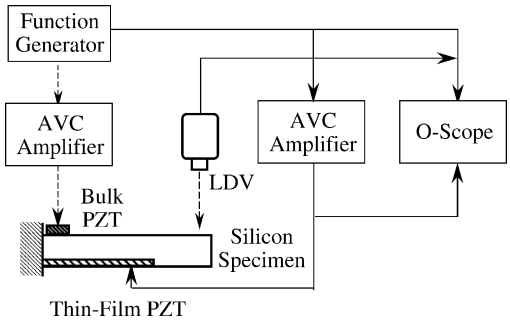

Fig. 11. Experimental setup to test actuation strength of the PZT thin film.

quencies of the test specimen. Fig. 9 shows the experimental setup. In this setup, the specimen is cantilevered at one end near the PZT film. The dimensions of the cantilever are 20 mm × 15 mm × 0.4 mm, whereas the size of the electrode (i.e., effective area of the PZT film) is 4 mm × 4 mm. The PZT film thickness is 1 μm, and the film capacitance is 35 nF. The corresponding dielectric constant is 237. A tiny piece of bulk PZT patch (roughly 3 mm × 3 mm in size) is also glued to the cantilever serving as a reference input. In this part of the experiment, a spectrum analyzer, together with an amplifier, drives the bulk PZT with swept sine to excite the specimen. A laser Doppler vibrometer (LDV) measures vibration of the specimen at the corner of the free end. The spectrum analyzer processes the PZT actuation voltage and LDV measurements to produce frequency response functions (FRF).

Fig. 10 shows the measured FRF, which reveals several major resonance peaks. A simple calculation from the classical plate theory indicates that the resonance peaks at 1.6 and 26 kHz are the first and third bending modes, respectively. The resonance peaks around 4.6 and 11 kHz are the first and second torsional modes, respectively. These vibration mode shapes have also been identified experimentally through modal analysis.

The second step is to demonstrate that the PZT thin-film actuator has enough actuation strength to perform active vibration control. Fig. 11 shows the experimental setup. First, a function generator drives the bulk PZT sinusoidally simulating a vibration disturbance input. Also, the LDV monitors the vibration of the cantilever. In the meantime, the function generator also drives the PZT thin-film actuator, with different phases and gains, to see if the PZT thin-film actuator has large enough actuation strength to offset the input vibration disturbance from the bulk PZT.

Fig. 12 shows the LDV response at 1.63 kHz (first bending mode resonance), when the PZT thin-film actuator is off. The first trace is the voltage from the function generator. The second trace is one-twentieth of the voltage into the bulk PZT. The third trace is one-twentieth of the voltage into the PZT thin film. The last trace is the measurement from LDV, whose sensitivity is 1 mm/s/V. Therefore, the velocity of the cantilever tip is around 0.3 mm/s, when the PZT thin film is off. Fig. 13 shows the LDV response at 1.63 kHz, when the PZT thin-film actuator is on with an 8 V actuation. The tip velocity is now significantly reduced to 0.1 mm/s. The results in Fig. 13 indicate that the PZT thin film is strong enough in serving as an actuator for active vibration control.

The third step of the test is to demonstrate the effectiveness of active vibration control via the PZT thin film. Fig. 14 shows the experimental setup. First, the spectrum analyzer generates a swept-sine excitation to the bulk PZT

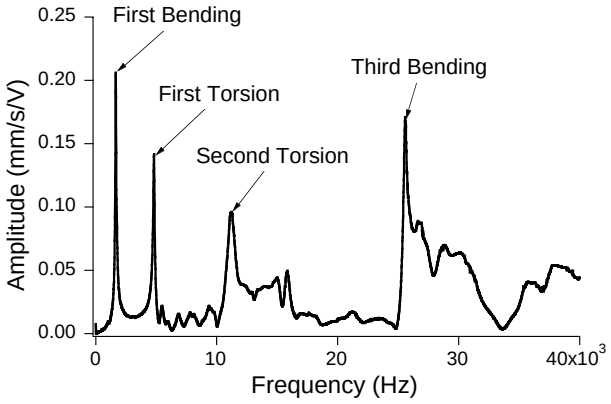

Fig. 10. Measured frequency response function of the silicon cantilever plate.

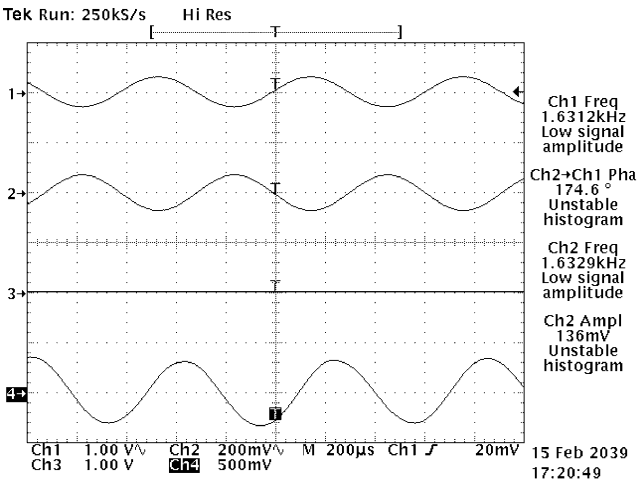

Fig. 12. Test results of film actuation strength at 1.63 kHz; PZT thin film is off.

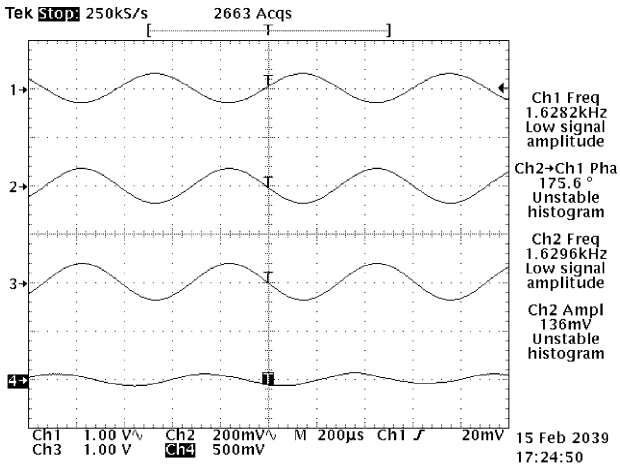

Fig. 13. Test results of film actuation strength at 1.63 kHz; PZT thin film is on.

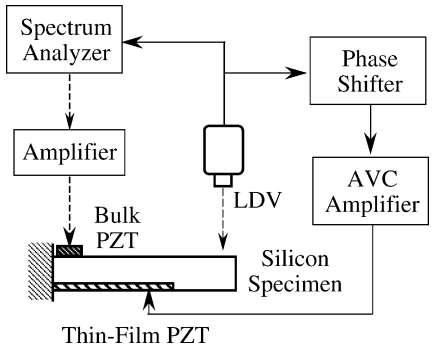

Fig. 14. Experimental setup for active vibration control.

serving as a vibration disturbance input. The LDV measurement is fed back to drive the PZT thin-film actuator with an AVC-780A01 phase shifter (made by PCB Piezotronics, Inc.) as the controller. In the meantime, the spectrum analyzer measures the FRF from the bulk PZT input excitation to the LDV measurement in order to monitor the effectiveness of the active vibration control.

Fig. 15 shows the measured FRF of the first bending mode with and without control. The control gain is 12, and the

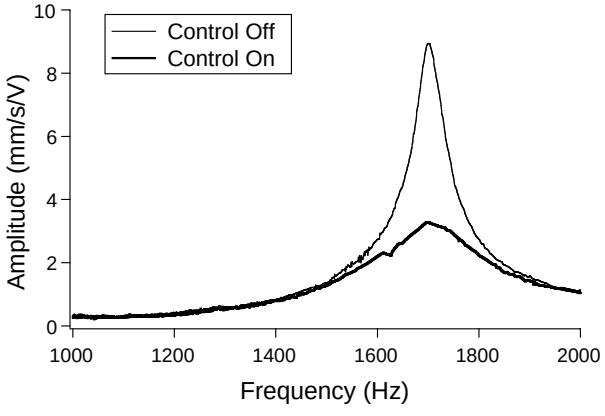

Fig. 15. FRF of the first bending mode with and without control.

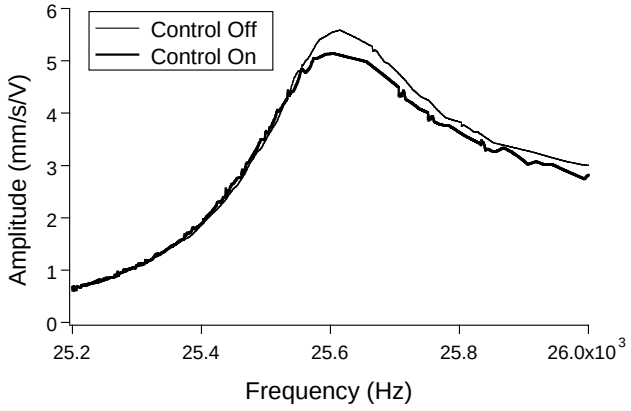

Fig. 16. FRF of the third bending mode with and without control.

controller shifts the phase angle in the range of 150–175°. When the control is off, the resonance amplitude is around 9 mm/s/V. When the control is on, the resonance amplitude is substantially reduced to 3 mm/s/V. Fig. 16 shows the measured FRF of the third bending mode with and without control. When the control is present, it reduces the resonance amplitude from 5.6 to 5 mm/s/V. Note that the PZT film is located near the cantilevered end, which experiences a significant curvature for the first, but not the third, bending mode. Therefore, the active vibration control is substantially more effective for the first bending mode.

6. Conclusions

We have developed a sol–gel process to fabricate PZT thin films with thickness of 2 μm in three coatings. The crack-free area can be as large as 5 mm × 5 mm. This is a substantial improvement over existing PZT films published in the literature.

The dielectric constant of the PZT films ranges from 200 to 400 depending on the batch tested. The piezoelectric constant d_{33} is around 120 pC/N. These numbers are comparable to those PZT films published in the literature.

PZT thin films can serve as a sensor measuring normal strain in the silicon substrate through use of a charge amplifier. The thin-film sensor can be calibrated using a laser vibrometer and Euler–Bernoulli beam theory.

Experimental measurements indicate that the PZT thin films can produce sufficient actuation strength to perform active vibration control. With the PZT thin film located near the cantilever end, the resonance amplitude of the first vibration mode can be reduced by 66% with a phase shifter serving as the controller.

Appendix A. Recipe of PZT sol

1. Dissolve 24.48 g Pb acetate in 16 g (15.2 ml) acetic acid.
2. Heat to 110 °C (10–15 min), cool to room temperature.

3. Mix 15.932 g (14.7 ml) Zr *n*-propoxide and 8.128 g (8.4 ml) Ti-isopropoxide.
4. Add to Pb solution the Zr + Ti mixture.
5. Add 16 g (16 ml) of deionized water.
6. Add 4 g (3.4 ml) lactic acid.
7. Add 6 g (4.8 ml) glycerol.
8. Add 4 g (3.6 ml) ethylene glycol.

References

[1] K. Suzuki, R. Maeda, J. Chu, T. Kato, M. Kurita, An active head slider using a piezoelectric cantilever for in-situ flying-height control, IEEE Trans. Magn. 39 (2003) 826–831.

[2] S.M. Sze, Semiconductor Sensors, Wiley, New York, 1994, Chapter 9.

[3] D.L. Polla, L.F. Francis, Processing and characterization of piezoelectric materials and integration into microelectromechanical systems, Annu. Rev. Mater. Sci. 28 (1998) 563–597.

[4] P. Muralt, Ferroelectric thin films for micro-sensors and actuators: a review, J. Micromech. Microeng. 10 (2000) 136–146.

[5] E.J. Seibel, M. Fauver, J. Crossman-Bosworth, Q.Y.L. Smithwick, C.M. Brown, Microfabricated optical fiber with microlens that produces large field-of-view, video rate, optical beam scanning for microendoscopy applications, in: I. Gannot (Ed.), Optical Fibers and Sensors for Medical Applications III, Proc. SPIE 4957 (2003) 46–55.

[6] P. Krulevitch, A.P. Lee, P.B. Ramsey, J.C. Trevino, J. Hamilton, M.A. Northrup, Thin film shape memory alloy microactuators, J. Microelectromech. 5 (1996) 270–282.

[7] N.A. Riza, D.L. Polla, W.P. Robbins, D.E. Glumac, High-resolution 50 nm linear displacement macroscale meander-line PZT actuator, Electron. Lett. 29 (1993) 1606–1608.

[8] P. Muralt, A. Kholkin, M. Kohli, T. Maeder, Piezoelectric actuation of PZT thin-film diaphragms at static and resonant conditions, Sens. Actuators A Phys. 53 (1996) 398–404.

[9] P. Luginbuhl, G.A. Racine, P. Lerch, B. Romanowicz, K.G. Brooks, N.F. deRooij, P. Renaud, Piezoelectric cantilever beams actuated by PZT sol–gel thin film, Sens. Actuators A Phys. 54 (1996) 530–535.

[10] P. Muralt, Piezoelectric thin films for MEMS, Integr. Ferroelectr. 17 (1997) 297–307.

[11] P. Luginbuhl, S.D. Collins, G.A. Racine, M.A. Gretillat, N.F. deRooij, K.G. Brooks, N. Setter, Microfabricated Lamb wave device based on PZT sol–gel thin film for mechanical transport of solid particles and liquids, J. Microelectromech. 6 (1997) 337–346.

[12] S.Y. Chen, C.L. Sun, Ferroelectric characteristics of oriented $Pb(Zr_{1-x}Ti_x)O_3$ films, J. Appl. Phys. 90 (2001) 2970–2974.

[13] H. Kueppers, T. Leuerer, U. Schnakenberg, W. Mokwa, M. Hoffmann, T. Schneller, U. Boettger, R. Waser, PZT thin films for piezoelectric microactuator applications, Sens. Actuators A Phys. 97 (8) (2002) 680–684.

[14] J.H. Feng, Colloidal processing, tape casting and sintering of PZT for development of piezoceramic/polymer interlayered composites, Ph.D. Dissertation, The University of Washington, 2000.

[15] T.S. Kim, D.J. Kim, J.K. Lee, H.I. Jung, Low temperature growth of PZT (52/48) thin films using RF magnetron sputtering method, in: Proceedings of the Symposium on Ferroelectric Thin Films V, Mater. Res. Soc, 1995, pp. 243–247.

[16] T. Hata, S. Kawagoe, W. Zhang, K. Sasaki, Y. Yoshioka, Proposal of new mixture target for PZT thin films by reactive sputtering, Vacuum 51 (1998) 665–671.

[17] R. Bruchhaus, D. Pitzer, R. Primig, M. Schreiter, W. Wersing, PZT thin films grown by multi-target sputtering: analysis of thin film stress, Integr. Ferroelectr. 21 (1998) 461–467.

[18] T. Sakoda, K. Aoki, S. Hashimoto, Y. Fukuda, Recent progress in sputtering PZT thin films for ferroelectric memories, Integr. Ferroelectr. 21 (1998) 385–396.

[19] I. Novotny, P. Sutta, F. Mika, V. Tvarozek, Piezoelectric ZnO thin films prepared by cyclic sputtering and etching technology, in: Proceedings of the 20th International Conference on Microelectronics, vol. 1, 1995, pp. 65–68.

[20] K. Eda, Y. Tomita, M. Sugimoto, A. Nanba, T. Ogura, Y. Taguchi, O. Kawasaki, Novel composite piezoelectric materials using direct bonding techniques, Proc. IEEE Ultrason. Symp. 2 (1995) 921–924.

[21] K. Eda, Y. Tomita, M. Sugimoto, T. Ogura, A. Nanba, Y. Taguchi, O. Kawasaki, Direct bonding of piezoelectric materials onto Si, in: Proceedings of the 10th IEEE International Symposium on Applications of Ferroelectrics, vol. 2, 1996, pp. 719–722.

[22] S.P. Beeby, N.M. White, Thick-film printed PZT actuator and polymer masking layers for micromachined silicon devices, in: Proceedings of the 10th Conference on Sensors and their Applications, 1999, pp. 131–136.

[23] R. Maas, M. Koch, N.R. Harris, N.M. White, A.G.R. Evans, Thick-film printing of PZT onto silicon, Mater. Lett. 31 (1997) 1–2.

[24] C.Y. Pan, Y.L. Chen, D.S. Tsai, Synthesis and properties of lead zirzonate titanate thin films via metalorganic chemical vapor deposition, J. Mater. Res. 17 (2002) 1536–1542.

[25] G. Yi, M. Sayer, Sol–gel processing of thick PZT films, in: Proceedings of the 8th IEEE International Symposium on Applications of Ferroelectrics, 1992, pp. 289–292.

[26] M.D. Liu, C.R. Lu, P.Y. Wang, Y.H. Rao, Y.K. Zeng, C.R. Li, Preparation of PZT ferroelectric thin films by sol–gel processing and their properties, Sens. Actuators A Phys. 49 (1995) 191–194.

[27] K.G. Brooks, I.M. Reaney, T. Maeder, N. Setter, Processing sol–gel PZT thin films for microactuators, Electroceramics, Verlag der Augustinus Buchhandlung, Aachen, Germany, vol. 2, 1994.

[28] W.I. Lee, J.K. Lee, I. Chung, C.W. Chung, I.K. Yoo, S.B. Desu, The characterization and electrical properties of doped PZT thin films prepared by sol–gel processing, in: Proceedings of the Fourth Symposium on Ferroelectric Thin Films, Mater. Res. Soc., 1995, 421–426.

[29] M. Sayer, G. Yi, M. Sedlar, Comparative sol gel processing of PZT thin films, Integr. Ferroelectr. 7 (1995) 1–4.

[30] L. Cakare, B. Malic, M. Kosec, Characterization of thick PZT 53/47 films prepared by sol–gel processing, in: Proceedings of 34th International Conference on Microelectronics, Devices and Materials, 1998, pp. 349–354.

[31] K. Miyazawa, K. Ito, R. Maeda, Structure and electrical properties of multilayer PZT films prepared by sol–gel processing, Ceram. Int. 26 (2000) 501–506.

[32] R. Dat, J.K. Lee, O. Auciello, A.I. Kingon, Pulse-laser ablation synthesis and characterization of layered $Pt/SrBi_2Ta_2O_9/Pt$ ferroelectric capacitors with practically no polarization fatigue, Appl. Phys. Lett. 67 (1995) 572–574.

[33] O. Auciello, R. Mamesh, Laser-ablation deposition and characterization of ferroelectric capacitors for nonvolatile memories, MRS Bull. 21 (1996) 31–36.

[34] Y.C. Hsu, Damping treatments for microstructures, Ph.D. Dissertation, The University of Washington, 2003.

[35] D.J. Jung, M. Dawber, A. Ruediger, J.F. Scott, H.H. Kim, K. Kim, Dielectric loss peak due to platinum electrode porosity in lead zirconate titanate thin-film capacitors, Appl. Phys. Lett. 81 (2002) 2436–2438.

[36] B. Vilquin, G. Le Rhun, R. Bouregba, G. Poullain, H. Murray, Effect of in situ Pt bottom electrode deposition and of Pt top electrode preparation on PZT thin films properties, Appl. Surf. Sci. 195 (2002) 63–73.

[37] S.H. Kim, D.Y. Park, H.J. Woo, D.S. Lee, J. Ha, Effects of IrO_2/Pt hybrid electrodes on the crystallization and ferroelectric performance of sol–gel-derived Pb(Zr, Ti)O_3 thin film capacitors, J. Mater. Res. 17 (2002) 1735–1742.

[38] A.J. Moulson, J.M. Herbert, Electroceramics, Chapman & Hall, 1990.
[39] W.L. Warren, D. Dimos, R.M. Waser, Degradation mechanisms in ferroelectric and high-permittivity perovskites, MRS Bull. 21 (1996) 40–45.
[40] K. Lefki, G.J.M. Dormans, Measurement of piezoelectric coefficients of ferroelectric thin films, J. Appl. Phys. 76 (1994) 1764–1767.
[41] D. Damjanovic, Stress and frequency dependence of the direct piezoelectric effect in ferroelectric ceramics, J. Appl. Phys. 82 (1997) 1788–1797.
[42] D. Damjanovic, Logarithmic frequency dependence of the piezoelectric effect due to pinning of ferroelectric–ferroelastic domain walls, Phys. Rev. B 55 (1997) R649–R652.
[43] E. Cattan, T. Haccart, G. Vélu, D. Rémiens, C. Bergard, L. Nicu, Piezoelectric properties of PZT films for microcantilever, Sens. Actuators A Phys. 74 (1999) 60–64.
[44] J.M. Vicente, B. Jimenez, Frequency dependence of the piezoelectric d_{31} coefficient as a function of ceramic tetragonality, Ferroelectrics (UK) 134 (1992) 157–162.
[45] M.A. Dubois, P. Muralt, Measurement of the effective transverse piezoelectric coefficient $e_{31,f}$ of AlN and $Pb(Zr_x, Ti_{1-x})O_3$ thin films, Sens. Actuators A Phys. 77 (1999) 106–112.
[46] A. Barzegar, D. Damjanovic, N. Ledermann, P. Muralt, Piezoelectric response of thin films determined by charge integration technique: substrate bending effects, J. Appl. Phys. 93 (2003) 4756–4760.
[47] J.F. Shepard Jr., P.J. Moses, S. Trolier-McKinstry, The wafer flexure technique for the determination of the transverse piezoelectric coefficient (d_{31}) of PZT thin films, Sens. Actuators A Phys. 71 (1998) 133–138.

Biographies

Yi-Chu Hsu is an Assistant Professor in the Department of Mechanical Engineering of Southern Taiwan University of Technology, Tainan, Taiwan. She received her BS degree in Harbour and River Engineering from National Taiwan Ocean University in Keelung, Taiwan, in 1992. She attended National Cheng Kung University in Tainan, Taiwan and received an MS degree in Hydraulic and Ocean Engineering, 1994. She spent 2 years as an Engineer at Hoshin Engineering Consultants Co. Ltd., Taipei, and another 2 years as a Research Engineer at National Taiwan University's Hydraulic Research Laboratory, Taipei, Taiwan. She attended the University of Washington at Seattle in year 1998 and received a PhD degree in Mechanical Engineering in year 2003. Her research interests include bio-MEMS and microfabrication.

Chia-Che Wu (Joseph) received an MSME degree from National Chung-Hsien University, Taiwan, in 1999. He is currently a PhD student in Mechanical Engineering Department of the University of Washington. His research interest is microelectromechanical systems using piezoelectric thin films.

Cheng-Chun Lee (Ryan) received a BSME degree from National Chiao-Tung University, Taiwan, in 1995, and an MS degree in Aeronautics and Astronautics Engineering from the University of Washington, Seattle, USA, in 2001. He is currently a PhD student in Mechanical Engineering Department of the University of Washington. His interest of study is MEMS.

G.Z. Cao (G.Z.) is an Associate Professor of Materials Science and Engineering and Mechanical Engineering at the University of Washington. He received his PhD from Eindhoven University of Technology in 1991, and MS from Shanghai Institute of Ceramics and BS from East China University of Technology. He was a Research Associate at the University of Twente and the University of Nijmegen, before moving to the United States and joined Advanced Materials Laboratory of the University of New Mexico and Sandia National Laboratories as a Senior Research Associate in 1995. In 1996, he was appointed to UW Faculty. Major awards include the European Union Research Fellowship in 1993, the College Outstanding Educator Award in 1999, and the University Distinguished Teaching Award in 2000. He has published over 120 refereed papers in a wide range of materials science field, edited two conference proceedings, and authored a book "Nanostructures and Nanomaterials: Synthesis, Properties and Applications".

I.Y. Shen (Steve) is a Professor of Mechanical Engineering Department of the University of Washington. He received his PhD degree in Mechanical Engineering from the University of California, Berkeley. His general research area is vibration, sensing, and actuation. In particular, his expertise includes PZT thin-film micro-sensors/actuators and spindle/rotor dynamics. In the areas of PZT thin films, he is developing micro-sensors and actuators for future medical devices. In the area of spindle and rotor dynamics, he is developing computational algorithms to predict vibration of complex rotating machines, such as hard disk drives and turbine engines. For his 12-year academic career in US, Professor Shen has published more than 50 archival journal papers in his field and more than 40 conference papers.